A discrete mode of endosomal GPCR signaling that does not require β-arrestin

Emily E. Blythe[1] and Mark von Zastrow[1-3]*

[1]Department of Psychiatry and Behavioral Sciences, University of California, San Francisco, San Francisco, CA, USA, [2]Department of Cellular and Molecular Pharmacology, University of California, San Francisco, San Francisco, CA, USA, [3]Quantitative Biology Institute, University of California, San Francisco, San Francisco, CA, USA *Correspondence: mark.vonzastrow@ucsf.edu

Abstract

The ability of GPCRs to initiate a second phase of G protein-coupled signaling after endocytosis is now well established. The prevailing current view is that GPCR signaling from endosomes is strictly dependent on β-arrestin. Here we revise this view by demonstrating that the vasoactive intestinal peptide receptor 1 (VIPR1), a family B GPCR, is able to internalize and initiate a distinct endosomal cAMP response in cells that completely lack β-arrestin. However, VIPR1 robustly recruits β-arrestin to both the plasma membrane and endosomes, and we show that β-arrestin recruitment plays a different role in temporally resolving plasma membrane and endosomal signaling phases into separate cAMP peaks. These results delineate a third endosomal GPCR signaling mode, distinguished by not requiring β-arrestin for its production, and reveal a discrete function of β-arrestin in sculpting the spatiotemporal cAMP response.

Introduction

G protein-coupled receptors (GPCRs) comprise the largest class of signaling receptors in animals, regulate essentially every physiological process, and are important drug targets[1]. Upon binding of an agonist, GPCRs engage cognate heterotrimeric G proteins to regulate specific downstream effectors [2,3]. The biochemical basis of GPCR activation has been studied to a level of atomic detail[4,5], but we are only now beginning to understand the subcellular organization of GPCR signaling[2,6,7]. Many GPCRs are not restricted to the plasma membrane and transit the endocytic pathway[8]. However, endocytosis was long believed only to impact the longer-term homeostatic regulation of GPCRs and not their acute signaling. Over the past several years, this view has changed due to accumulating evidence that GPCRs can engage G proteins after endocytosis and leverage the endocytic network to promote, as well as attenuate, cellular responses[2,7].

Support for this emerging view is particularly well-developed for signaling mediated by GPCRs that couple to stimulatory heterotrimeric G proteins (G_s) and activate adenylyl cyclases to produce cAMP. A number of such GPCRs have now been shown to engage G_s on the endosome limiting membrane as well as the plasma membrane and stimulate sequential phases of cAMP production from both locations[9–19]. It is increasingly clear that GPCRs vary considerably in the magnitude and duration of cAMP production that they stimulate from endomembranes compared to the plasma membrane[9,10,12,13,16,17,20]. Such differences have been clearly shown to impact

46 downstream cellular responses mediated by GPCRs, both at the cell and tissue
47 levels[9,11,13,15,16,18,19,21], but relatively little is known about how such signaling diversity is
48 programmed.
49
50 The present understanding holds that endosomal signaling by GPCRs is strictly dependent on β-
51 arrestin, and that receptor-specific signaling is programmed according to overall stability of the
52 GPCR / β-arrestin complex[2,17,20]. Some GPCRs require binding to β-arrestin for internalization
53 and then remain bound, using β-arrestin as a molecular scaffold to stabilize receptors together
54 with other signaling proteins on the endosome limiting membrane[20,22,23]. This 'class B' behavior
55 typically results in a sustained cAMP elevation[12,13,17,20,23–25]. Other GPCRs similarly require β-
56 arrestin to internalize, but then dissociate from β-arrestin during or shortly after endocytosis[22].
57 This 'class A' behavior is still β-arrestin-dependent, due to β-arrestin being needed to internalize,
58 but receptors dissociated from β-arrestin transit endosomes rapidly and produce a transient cAMP
59 response[11,16,17,20].
60
61 It has long been known that some GPCRs do not require β-arrestin for endocytosis[26]. In principle,
62 therefore, there might exist an additional mode of GPCR signaling from endosomes that does not
63 strictly require β-arrestin. We became curious about this possibility based on previous studies
64 reporting that the vasoactive intestinal peptide receptor 1 (VIPR1 or VPAC1), a secretin-subfamily
65 GPCR, internalizes in a β-arrestin-independent manner yet robustly recruits β-arrestin[27,28]. Here
66 we show that this distinct cell biology defines a third mode of endosomal GPCR signaling and
67 illustrates a discrete function of β-arrestin in sculpting the spatiotemporal cAMP response
68 independent of its prototypical endocytic function.
69
70
71 **Results**
72
73 *VIPR1 mediates sequential phases of cAMP production from the plasma membrane and*
74 *endosomes*
75
76 To begin to characterize VIPR1 signaling, we first assessed the endogenous vasoactive intestinal
77 peptide (VIP) -elicited cAMP response in HEK293 cells using a genetically encoded fluorescent
78 biosensor, cADDis, which enables real time readout in living cells at 37˚C. VIP stimulated a
79 complex cAMP response, characterized by a sharp peak of cAMP elevation that desensitized
80 over ~5 minutes followed by a second, lower-level cAMP peak and then a plateau of cAMP
81 elevation that persisted above baseline in the prolonged presence of VIP (**Fig 1A**). To investigate
82 if endocytosis impacts this complex cAMP response, we examined the effect of experimentally
83 imposing endocytic blockade. Preventing endocytosis using a chemical inhibitor of dynamin,
84 Dyngo4a, abolished the second peak and subsequent plateau without detectably affecting the
85 first peak (**Fig 1A**, blue curve). Genetically imposing endocytic inhibition by expressing a
86 dominant-negative mutant version of dynamin (Dyn1-K44E) also selectively blocked the second
87 signaling phase (**Fig 1B**). These results suggest that the VIP-elicited cAMP response is
88 composed of two phases: a first peak from the plasma membrane, and a second peak and plateau
89 from endosomes.

We next sought to identify the receptor(s) responsible for mediating this biphasic VIP-elicited cAMP response. VIPR1 (VPAC1) is the main VIP-sensitive GPCR natively expressed in HEK293 cells[28–30]. By generating CRISPR-knockout cell clones and measuring the VIP-elicited cAMP response, we verified that VIPR1 indeed mediates both cAMP signaling phases (**Supp Fig 1**).

VIPR1 was previously shown to localize both to the plasma membrane and endosomes in HEK293 cells[28], but the subcellular location(s) of ligand-dependent VIPR1 and G_s activation have not been determined. To investigate this, we used conformational biosensors to detect either active-state VIPR1 (mini-G_s)[31,32] or a conformational intermediate in the process of G_s activation (Nb37)[14,33]. We detected recruitment of each biosensor specifically to the plasma membrane or endosome limiting membrane using an enzyme complementation (NanoBiT) bystander assay. VIP promoted recruitment of both biosensors to the plasma membrane and then to endosomes (**Fig 1C**). These results suggest that VIP-induced activation of VIPR1 and G_s occurs at both membrane locations, sequentially and with kinetics consistent with the biphasic cytoplasmic cAMP elevation measured using the cAMP biosensor.

VIPR1 endocytosis is β-arrestin-independent despite agonist-induced β-arrestin recruitment to both the plasma membrane and endosomes

The ability of VIPR1 to signal from endosomes was not surprising because such behavior has been shown previously for other family B GPCRs[10,12,15,20]. However, a novel feature of VIPR1 is that its endocytosis is thought not to require β-arrestin, despite VIPR1 having the ability to recruit β-arrestin both to the plasma membrane and endosomes after agonist-induced activation[27,28]. As the experimental evidence supporting this distinction is presently limited to insensitivity to overexpressed dominant negative β-arrestins, we sought to independently test if β-arrestin is required for VIPR1 endocytosis in a true genetic null. To do so, we generated two independent β-arrestin1 and 2 double-knockout (βarr1/2 DKO) cell lines using CRISPR. We validated complete knockout by genomic DNA sequencing, western blotting and then functionally using the agonist-induced internalization of the β2-adrenergic receptor (β2AR) as a representative β-arrestin-dependent process (**Supp Fig 2**).

To examine VIPR1 internalization, we used a cell-impermeant HaloTag dye (JF_{635}i-HTL) to selectively label receptors in the plasma membrane of living cells[34]. HaloTag-VIPR1 labeled at 37˚C localized both to the plasma membrane and intracellular puncta that were defined as early endosomes by colocalization with DsRed-labeled EEA1 (**Fig 2A-B**). Similar results were observed using FLAG-VIPR1 and anti-FLAG antibody labeling of surface receptors (**Fig 2C**). Pearson correlation analysis indicated that VIP increased the degree of VIPR1 internalization (**Fig 2B**), and this was also observed by flow cytometry (**Supp Fig 3**). However, internalization was also detectable in cells to which VIP was not added, as well as after the addition of a competitive VIPR1 antagonist, VIP(6-28)[35] (**Fig 2A-B**), suggesting that VIPR1 internalization has both agonist-induced and agonist-independent components. Nevertheless, VIPR1 internalization clearly still

occurred in βarr1/2 DKO cells (**Fig 2A-B, Supp Fig 4A-B**), despite being strongly inhibited by Dyngo4a (**Fig 2A-B**) and mutant dynamin (**Fig 2C-D**).

Our demonstration that VIPR1 endocytosis is indeed β-arrestin-independent prompted us to re-evaluate if VIPR1 recruits β-arrestin. We observed recruitment of mApple-labeled β-arr1 to the plasma membrane followed by endosomes using fluorescence microscopy (**Fig 3A**), and further confirmed recruitment to these locations using the NanoBiT protein complementation assay (**Fig 3B-C**). Altogether, the above results clearly establish that VIPR1 is unique in two ways relative to all other GPCRs previously established to signal from endosomes. First, VIPR1 does not require β-arrestin to undergo dynamin-dependent endocytosis. Second, despite not requiring β-arrestin to internalize, VIPR1 recruits β-arrestin to both the plasma membrane and to endosomes in response to agonist-induced activation.

A discrete role of β-arrestin in temporally resolving the VIPR1-mediated signaling phases

If β-arrestin binds active VIPR1 but is not necessary for receptor endocytosis, what role does it play in signaling? To investigate this, we first compared endogenous VIPR1-mediated cAMP signaling produced in β-arr1/2 DKO cells to that produced in the parental (wild type) cell background. In β-arr1/2 DKO cells, VIP still produced a transient cAMP peak (**Fig 4A, Supp Fig 5A**), but this peak was more prolonged when compared to that observed in parental wild type cells (**Fig 1A**). We did not observe a distinct, second cAMP peak in β-arr1/2 DKO cells, but a prolonged plateau above baseline was still observed. This contrasts with a complete loss of the prolonged cAMP plateau after endocytic inhibition (**Supp Fig 5B**). Further, VIP-induced endosomal recruitment of both mini-Gs and Nb37 was still observed in β-arr1/2 DKO cells (**Fig 4B-C, Supp Fig 5C-D**). Together, these results suggest that β-arrestins are not required for VIPR1-mediated signaling from either the plasma membrane or endosomes, but that β-arrestins affect response kinetics.

To further investigate the effect of β-arrestin on the biphasic VIPR1-mediated cAMP response, we pursued genetic rescue in β-arr1/2 DKO cells using recombinant β-arrestin (β-arr2-mApple) expressed under tetracycline-inducible control (DKO-R, **Supp Fig 6**). Doxycycline-induced overexpression of β-arrestin (+Dox) accelerated desensitization of the first phase of VIP-induced cytoplasmic cAMP elevation relative to the uninduced (-Dox) condition (**Fig 5A, Supp Fig 7A**). A distinct, second cAMP peak was not evident in the uninduced condition but became evident after doxycycline rescue. The magnitude of the following cAMP plateau, however, was unaffected by β-arrestin overexpression. Nevertheless, this plateau remained endocytosis-dependent because it was blocked by Dyngo4a irrespective of the rescue condition (**Fig 5B, Supp Fig 7B**). Together, these results verify that β-arrestin is not necessary for VIPR1-mediated signaling from endosomes and indicate that β-arrestin plays a different role in resolving the sequential signaling phases into temporally separated peaks of cAMP elevation.

Discussion

The present findings take advantage of the unique trafficking properties of VIPR1 to reveal a novel mode of GPCR signaling from endosomes and a discrete signaling function of β-arrestin. cAMP signaling from endosomes was initially recognized through the study of 'class B' GPCRs that remain stably bound to β-arrestin after endocytosis[12,13,17,20,23–25]. A second mode of endosomal cAMP signaling was then identified for 'class A' GPCRs that dissociate from β-arrestin during or immediately after endocytosis[11,16]. For both of these previously delineated modes, the signal from endosomes is inherently dependent on β-arrestin because β-arrestin is required for receptors to internalize. VIPR1 is a class B GPCR according to its β-arrestin recruitment properties[22,28], but it defines a distinct, third mode of endosomal cAMP signaling in which β-arrestin is not necessary either for internalization or for generating the endosomal signal. VIPR1 further reveals a discrete signaling function of β-arrestin. Rather than being required to generate the endosomal signal, β-arrestin enables sequential peaks of receptor / G protein activation initiated from different subcellular locations – the plasma membrane and endosomes – to be resolved into temporally separated peaks of global cytoplasmic cAMP elevation. Accordingly, this third mode of endosomal signaling is β-arrestin-independent and reveals a discrete function of β-arrestin in sculpting the spatiotemporal profile of cellular GPCR signaling (**Fig 6**).

The ability of GPCRs to selectively engage one endosomal signaling mode relative to another has intriguing implications for the cellular logic of GPCR signaling. In particular, we note that each mode enables different GPCRs to produce different temporal signaling profiles using the same second messenger. The class B mode results in GPCRs producing a sustained cytoplasmic cAMP elevation, whereas the class A mode results in a transient peak followed by a plateau. The third mode, as delineated here, results in the production of two cAMP peaks in close succession followed by a plateau. Accordingly, we speculate that GPCR-specific endosomal signaling modes could enable cells to accurately communicate the nature of distinct chemical cues sensed by different GPCRs through a common downstream intermediate.

Methods

Cell culture

HEK293 (ATCC CRL-1573) were cultured in Dulbecco's modified Eagle's medium (DMEM, Gibco 1196511) supplemented with 10% FBS (Hyclone SH30910.03). All knockout and stable cell lines used in this study were derived from this HEK293 cell line. Cells stably expressing FLAG-VIPR1 were selected using 500 µg/mL geneticin, and cells stably expressing HaloTag-VIPR1 or HaloTag-β2AR were selected using 25 µg/mL zeocin. Monoclonal β-arr1/2 DKO cell lines stably expressing β-arr2-mApple were selected using 2 µg/mL puromycin and screened for inducible expression by flow cytometry. Rescue was induced 24 hours before experiments, unless otherwise noted, using 1 ug/mL doxycycline. All cells were routinely checked for mycoplasma contamination (MycoAlert, Lonza).

DNA constructs

Information on all plasmids used in this study can be found in **Supp Table 1**. Lipofectamine 2000 (Thermo Fisher) was used for transfections according to the manufacturer's protocol.

221
222 *Generation of CRISPR knockout cell lines*
223 sgRNAs (**Supp Table 2**) were designed using the Synthego CRISPR design tool. To make RNP,
224 3 µL total of 53.3 µM sgRNA (Synthego) was mixed with 2 µL of 40 µM Cas9 (UC Berkeley
225 Macrolab), and the mixture was incubated at room temperature for 10 minutes. Electroporation of
226 the RNP complex was carried out using the SF Cell Line 4D-Nucleofector kit (Lonza) and program
227 CM-130 with 2.0×10^5 cells. Genetic modifications of monoclonal cell lines were verified from
228 genomic PCR amplicons (**Supp Table 2**) using Sanger sequencing in combination with the
229 Synthego ICE Analysis Tool or by next generation sequencing (Amplicon-EZ, Azenta Life
230 Sciences). Loss of β-arr1/2 expression was further confirmed by western blot (anti-β-arr1/2: Cell
231 Signaling Technologies 4674; anti-α-tubulin: Cell Signaling Technologies 3873). For the β-arr1/2
232 DKO531 cell line, ARRB1 and ARRB2 modifications were done simultaneously, while for the β-
233 arr1/2 DKO836 cell line, modifications were done sequentially.
234
235 *cADDis microplate cAMP assay*
236 Real-time intracellular cAMP was measured using the Green Up cADDis cAMP biosensor
237 (Montana Molecular), as described previously[36]. Briefly, cells were treated with cADDis BacMam
238 and plated into 96-well plates (Corning 3340). After 24 hours, cells were washed with assay buffer
239 (20 mM HEPES pH 7.4, 135 mM NaCl, 5 mM KCl, 0.4 mM $MgCl_2$, 1.8 mM $CaCl_2$, 5 mM d-glucose)
240 twice before a 10 minute incubation in a 37°C plate reader (Synergy H4, BioTek), optionally with
241 DMSO or Dyngo4a (30 µM, Abcam ab120689) as indicated in figure legends. Fluorescence was
242 read at an excitation wavelength of 500 nm and an emission wavelength of 530 nm every 20-30
243 seconds for 35 minutes, with vehicle or agonist added after 5 minutes. Change in intracellular
244 cAMP ($\Delta F / F_0$) was calculated as the change in fluorescence ($\Delta F = F - F_0$) normalized to the
245 average of the 5 minute baseline (F_0).
246
247 *cADDis live epifluorescence microscopy*
248 Cells were transfected with the appropriate constructs 48 hours prior to experiments and plated
249 into glass bottom dishes (MatTek Corporation) coated with 0.001% (w/v) poly-L-lysine (Millipore
250 Sigma). Cells were washed three times with assay media (DMEM, no phenol red, 30 mM HEPES
251 pH 7.4) before imaging. Imaging was conducted using a Nikon TE2000 inverted microscope fitted
252 with a Nikon 20x/0.7 NA objective, Sutter Lambda HPX-L5 LED epifluorescence illuminator, Sutter
253 excitation / emission filter wheels and Point Grey CMOS camera controlled by Micromanager[37]
254 (www.micro-manager.org). A dual channel dichroic filter set (Chroma 89021) was used to
255 separately acquire cADDis (470/40 excitation, 520/50 emission) and mCherry (572/35 excitation,
256 632/60 emission) fluorescence signals. Cells were maintained at 37˚C during image collection
257 using a custom-built heated stage and stage top incubator. 1 µM VIP was added after a 2 minute
258 baseline, and forskolin (Fsk, 10 µM, MilliporeSigma) and 3-isobutyl-1-methylxanthine (IBMX, 500
259 µM, MilliporeSigma) were added 30 minutes later. Data was processed using Cell Profiler 4[38]
260 (www.cellprofiler.org). Briefly, cells were identified using the mCherry channel, and the intensity
261 of the cADDis channel was measured over the entire image and in the cell mask. Each frame was
262 background corrected by subtracting the lower quartile fluorescence intensity of the entire image.
263 The normalized change in fluorescence of the cell mask was calculated as $(F - F_0)/(F_{FskIBMX} - F_0)$,
264 where F_0 is the average fluorescence over the first two minutes and $F_{FskIBMX}$ is the average

265 fluorescence of the final two minutes. Each biological replicate is the average of 1-2 dishes of
266 approximately 20-30 cells per dish.
267
268 *NanoBiT luciferase complementation assays*
269 Cells grown in 6-well plates were transfected with HaloTag-VIPR1 and the appropriate
270 LgBit/SmBiT constructs 24 hours prior to experiments. Experiments using the Nb37-SmBiT(101)
271 construct also required the cotransfection of a tricistronic G protein construct (human Gβ1, bovine
272 Gγ1, and human Gαs). For the assay, cells were lifted and centrifuged at 500 x g for 3 minutes.
273 Cells were resuspended in assay buffer supplemented with 5 μM coelenterazine-H (Research
274 Products International) to a concentration of $5x10^5$ or $1x10^6$ cells/mL, and 100 μL of cells were
275 plated into untreated white 96-well plates (Corning 3912). Plates were incubated at 37 °C and 5%
276 CO_2 for 30 minutes prior to the assay. Luminescence was read on a plate reader (Synergy H4,
277 BioTek) prewarmed to 37 °C. After a 5 minute baseline reading, vehicle or agonist were added at
278 concentrations indicated in figure legends, and luminescence was read for another 30 minutes.
279 To calculate the change in luminescence, each well was first normalized to its average baseline
280 luminescence (ΔLuminescence). For normalization, the average change in luminescence for
281 vehicle-treated samples was subtracted from the average change in luminescence for drug-
282 treated samples ($\Delta Luminescence_{VIP\text{-}vehicle}$).
283
284 *Confocal microscopy*
285 All fixed and live confocal imaging was carried out using a Nikon Ti inverted microscope fitted with
286 a CSU-22 spinning disk unit (Yokogawa), custom laser launch (100 mW at 405, 488, 561, and
287 640 nm, Coherent OBIS), Sutter emission filter wheel and Photometrics Evolve Delta EMCCD
288 camera. Samples were imaged using an Apo TIRF 100x/1.49 NA oil objective (Nikon).
289
290 For live imaging, cells were transfected with the appropriate constructs 48 hours prior to
291 experiments and plated into glass bottom dishes (Cellvis) coated with 0.001% (w/v) poly-L-lysine
292 (Millipore Sigma). For surface labeling of receptor, cells were incubated with either monoclonal
293 anti-FLAG M1 antibody (Millipore Sigma F3040) labeled with Alexa Fluor 647 (Thermo Fisher
294 A20186) or 200 nM JF_{635}i-HTL[34] for 10 minutes at 37 °C and 5% CO_2. After three washes, cells
295 were imaged in assay media (DMEM, no phenol red, 30 mM HEPES pH 7.4) in a temperature-
296 and humidity-controlled chamber (Okolab). For time-lapse, cells were imaged at 20 second
297 intervals for 22 minutes, with 500 nM VIP added after 2 minutes.
298
299 For fixed imaging, cells were transfected with the appropriate constructs 48 hours prior to
300 experiments and plated onto coverslips (Fisher Scientific 12-545-100P) coated with 0.001% (w/v)
301 poly-L-lysine (Millipore Sigma). Coverslips were washed with assay media (DMEM, no phenol
302 red, 30 mM HEPES pH 7.4), and some were pretreated with Dyngo4a (30 μM, Abcam ab120689)
303 or VIP(6-18) (2.5 μM, Tocris 1905) for 10 minutes prior to labeling with 200 nM JF_{635}i-HTL for 10
304 minutes at 37 °C and 5% CO_2. Vehicle or 500 nM VIP was added for 20 minutes, followed by
305 washes with PBS and fixation in 3.7% formaldehyde (Fisher, F79) in modified BRB80 (80 mM
306 PIPES pH 6.8, 1 mM MgCl2, 1 mM CaCl2) for 20 minutes. Coverslips were mounted on glass
307 slides using ProLong Gold Antifade mounting media (Invitrogen P10144).
308

309 All image analysis was carried out in Cell Profiler 4[38], and all images for figures were processed
310 using Fiji[39]. For colocalization analysis, the Pearson's correlation coefficient was calculated in
311 individual cells segmented manually. For intracellular puncta counting, cells were first segmented
312 automatically using the mCherry channel, followed by a manual ROI adjustment if necessary.
313 Puncta were then automatically identified using the JF_{635}i-HTL or Alexa Fluor 647 channels, and
314 intracellular puncta within a shrunken ROI to eliminate plasma membrane artifacts were counted.
315
316 *Receptor internalization by flow cytometry*
317 All experiments were carried out using cell lines stably expressing an N-terminal HaloTag fusion
318 of the receptor of interest. Agonist or vehicle was added to cells grown in 12-well plates coated
319 with 0.001% (w/v) poly-L-lysine (Millipore Sigma) and incubated at 37 °C and 5% CO_2 as indicated
320 in figure legends. At the end of the incubation, plates were cooled on ice for 10 minutes, and all
321 subsequent steps were carried out on ice. JF_{635}i-HTL was added to a final concentration of 200
322 nM, and after a 30 minute incubation, the media was aspirated and replaced with assay media
323 (DMEM, no phenol red, 30 mM HEPES pH 7.4) containing 400 nM JFX_{549}-HTL[40] for another 30
324 minutes. Cells were washed twice with DPBS, and assay media was added for a 30 minute
325 washout period. After washing cells once with PBS-EDTA (UCSF Cell Culture Facility), cells were
326 lifted with 100 uL of TrypLE Express (Thermo Fisher) at room temperature for 10 minutes. TrypLE
327 was quenched with 150 uL PBS-EDTA + 2.5% FBS, and resuspended cells were transferred into
328 an untreated black 96-well plate (Corning). Data from 10,000 events was collected on an Attune
329 NxT Flow Cytometer equipped with a CytKick Autosampler (Thermo Fisher). JFX_{549}-HTL and
330 mApple were measured using a 561 nm excitation laser and a 585/16 nm emission filter, while
331 JF_{635}i-HTL was measured with a 637 nm excitation laser and a 670/14 nm emission filter. Data
332 were analyzed using FlowJo v10.8 Software (BD Life Sciences). Populations were gated for only
333 cells expressing detectable levels of receptor in all channels, and surface receptor was calculated
334 as a ratio of the medians of fluorescence (JF_{635}i / JFX_{549}).
335
336 *Statistical analysis and reproducibility*
337 All data are shown as individual biological replicates or as a mean or median ± standard deviation
338 from at least 3 biologically independent experiments. Each biological replicate in the cAMP,
339 NanoBiT, and flow cytometry assays represents the average of at least two technical replicates,
340 and all images are representative of at least 3 biologically independent experiments. Statistical
341 tests were carried out using Prism 8 (GraphPad) as noted in figure legends.
342
343 **Acknowledgements**
344
345 We thank D. Gordon and A. Ehrlich for assistance with CRISPR; L. Lavis for helpful discussion
346 and sharing reagents; A. Inoue, G. Schulte, R. Irannejad, and A. Marley for sharing constructs; B.
347 Barsi-Rhyne and the rest of the von Zastrow lab for helpful discussion; and the following core
348 facilities for providing services to support this research: the UCSF Center for Advanced Light
349 Microscopy (K. Herrington, S. Kim, and D. Larsen), the UCSF Center for Advanced Technology
350 (E. Chow), and the UCSF Helen Diller Family Comprehensive Cancer Center Laboratory for Cell
351 Analysis (S. Elmes; supported by the National Institutes of Health under award P30CA082103).
352 These studies were supported by grants from the National Institutes of Health National Cancer

Institute (F32CA260118 to E.E.B.), National Institute on Drug Abuse (DA010711 and DA012864 to M.v.Z.) and National Institute of Mental Health (MH120212 to M.v.Z.).

Author Contributions

E.E.B. and M.v.Z. conceived of and designed the research. E.E.B. carried out experiments and analyzed data. E.E.B. and M.v.Z. wrote the paper.

Competing Interests

The authors declare no competing interests.

365 **Figures**

366

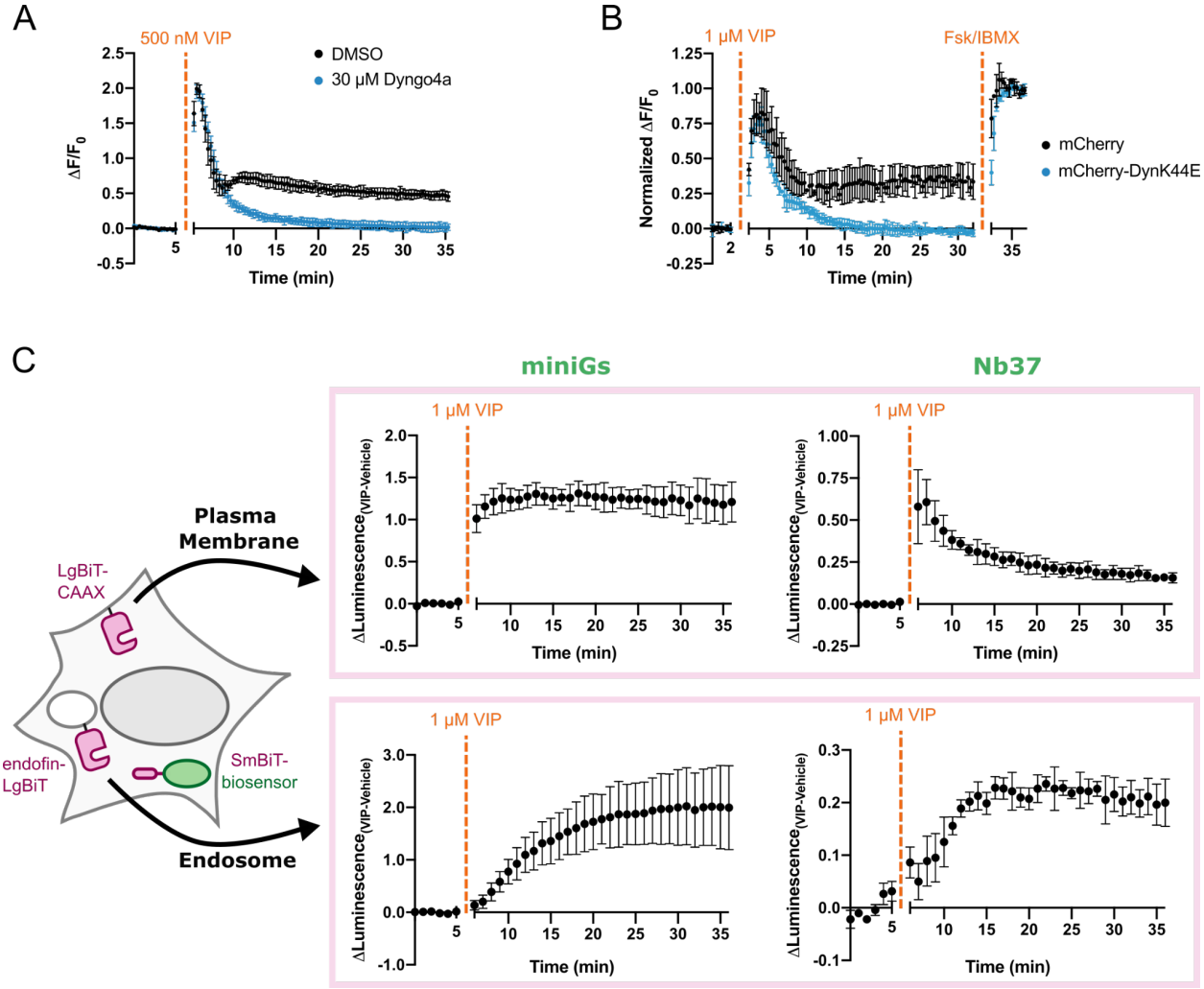

367

368

369 **Figure 1.** VIPR1-induced cAMP signaling is biphasic. (A) Fluorescence change of cADDis cAMP
370 biosensor upon treatment with 500 nM VIP added at 5 minutes. Cells were pretreated with 30 μM
371 Dyngo4a or DMSO for 10 minutes. (B) Fluorescence change of cADDis in cells expressing
372 dominant negative dynamin 1 (mCherry-DynK44E) or mCherry upon treatment with 1 μM VIP
373 added at 2 minutes. Fluorescence was measured by microscopy and normalized to fluorescence
374 change upon co-application of forskolin (Fsk, 10 μM) and IBMX (500 μM) at 32 minutes. (C)
375 NanoBiT bystander assays showing recruitment of SmBiT-miniGs (left panels) and Nb37-SmBiT
376 (right panels) to the plasma membrane (LgBiT-CAAX, top panels) and the endosome (endofin-
377 LgBiT, bottom panels), as measured by a change in luminescence upon addition of 1 μM VIP at
378 5 minutes. For all data, n ≥ 3 and error bars are S.D.

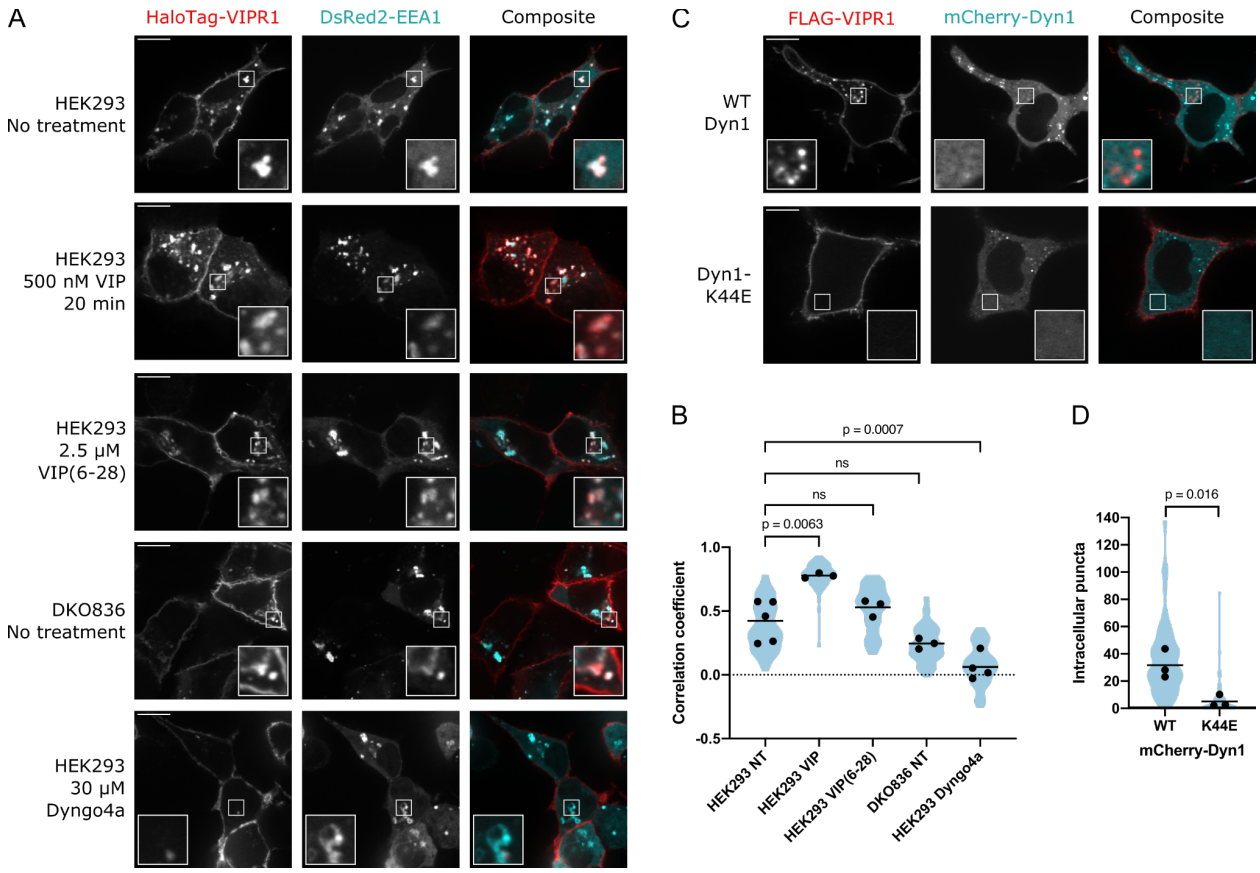

Figure 2. VIPR1 is internalized in a β-arrestin-independent and dynamin-dependent manner. (A) Cells coexpressing HaloTag-VIPR1, labeled with cell-impermeant JF_{635}i-HTL for 10 minutes, and DsRed2-EEA1 underwent the noted treatments before fixation and imaging. Scale bar is 10 μm. (B) Quantification of fixed imaging in (A). Cells were manually segmented, and the correlation coefficient was calculated for each cell. Mean correlation coefficients are shown for each biological replicate (9-31 cells), with a line at the mean of means and cell-level data superimposed as a violin plot. Significance was determined by a one-way ANOVA with Dunnett's multiple comparisons test. (C) HEK293 cells were co-transfected with FLAG-VIPR1 and either WT or mutant mCherry-Dyn1. Cells were labeled with anti-FLAG M1 conjugated with Alexa Fluor 647 for 10 minutes before live imaging. (D) Quantification of live imaging in (C). Intracellular puncta per cell were identified and counted using an automated pipeline in CellProfiler. Median counts are shown for each biological replicate (18-32 cells), with a line at the mean of medians and cell-level data superimposed as a violin plot. Significance was determined by an unpaired t-test.

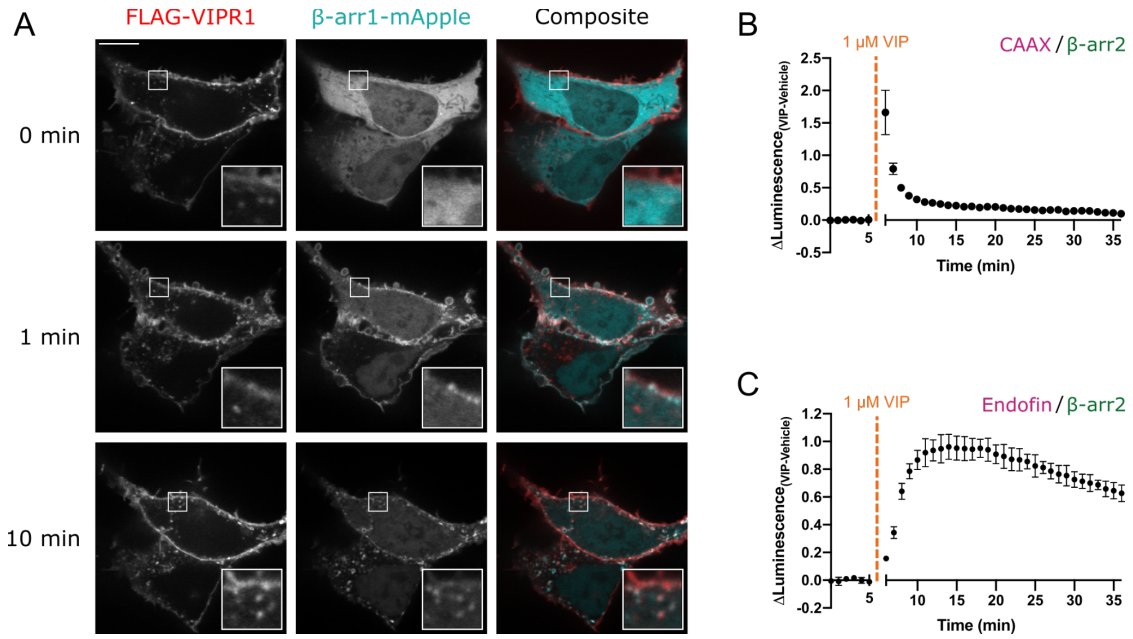

Figure 3. β-arrestin is recruited to activated VIPR1 at the plasma membrane and endosomes. (A) Representative stills from time-lapse microscopy of co-expressed FLAG-VIPR1 and β-arr1-mApple, with 500 nM VIP added at t = 0 minutes. Surface FLAG-VIPR1 was labeled with anti-FLAG M1 antibody conjugated to Alexa Fluor 647 for 10 minutes before imaging. Scale bar is 10 μm. (B, C) Change in luminescence in cells coexpressing β-arr2-smBiT and LgBiT-CAAX (B) or endofin-LgBiT (C) upon addition of 1 μM VIP at 5 minutes. For both panels, n ≥ 3 and error bars are S.D.

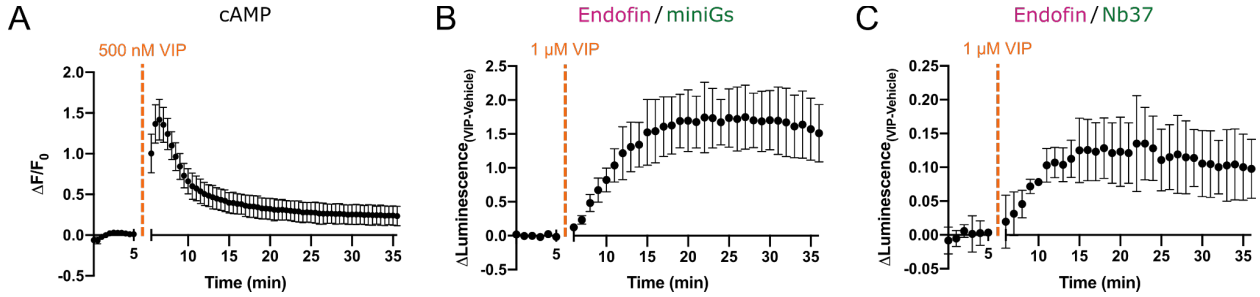

Figure 4. β-arrestin is dispensable for VIPR1 endosomal cAMP signaling. (A) Fluorescence change of cADDis in β-arr1/2 DKO line (DKO836) upon treatment with 500 nM VIP added at 5 minutes (B,C) Change in luminescence in DKO836 cells with endofin-LgBiT and SmBiT-miniGs (B) or Nb37-SmBiT (C) upon addition of 1 μM VIP at 5 minutes. For all data, n ≥ 3 and error bars are S.D.

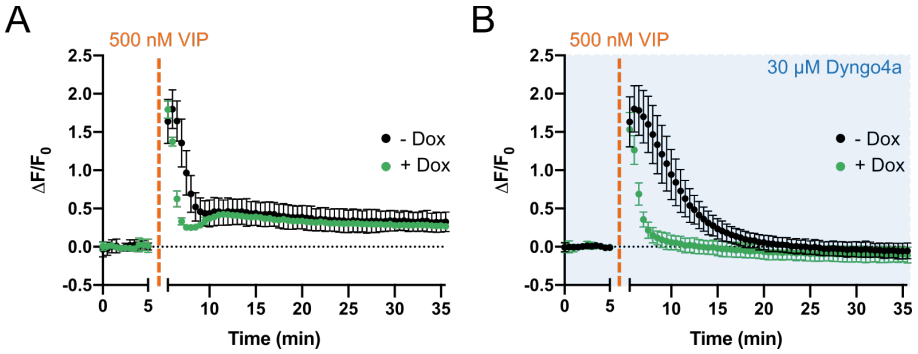

Figure 5. β-arrestin resolves phases of cAMP signaling. Fluorescence change of cADDis in DKO836-R upon treatment with 500 nM VIP added at 5 minutes. Cells were pretreated with DMSO (A) or 30 μM Dyngo4a (B) for 10 minutes. Cells treated with Dox to induce expression of β-arr2-mApple are shown in green, n ≥ 3, and error bars are S.D.

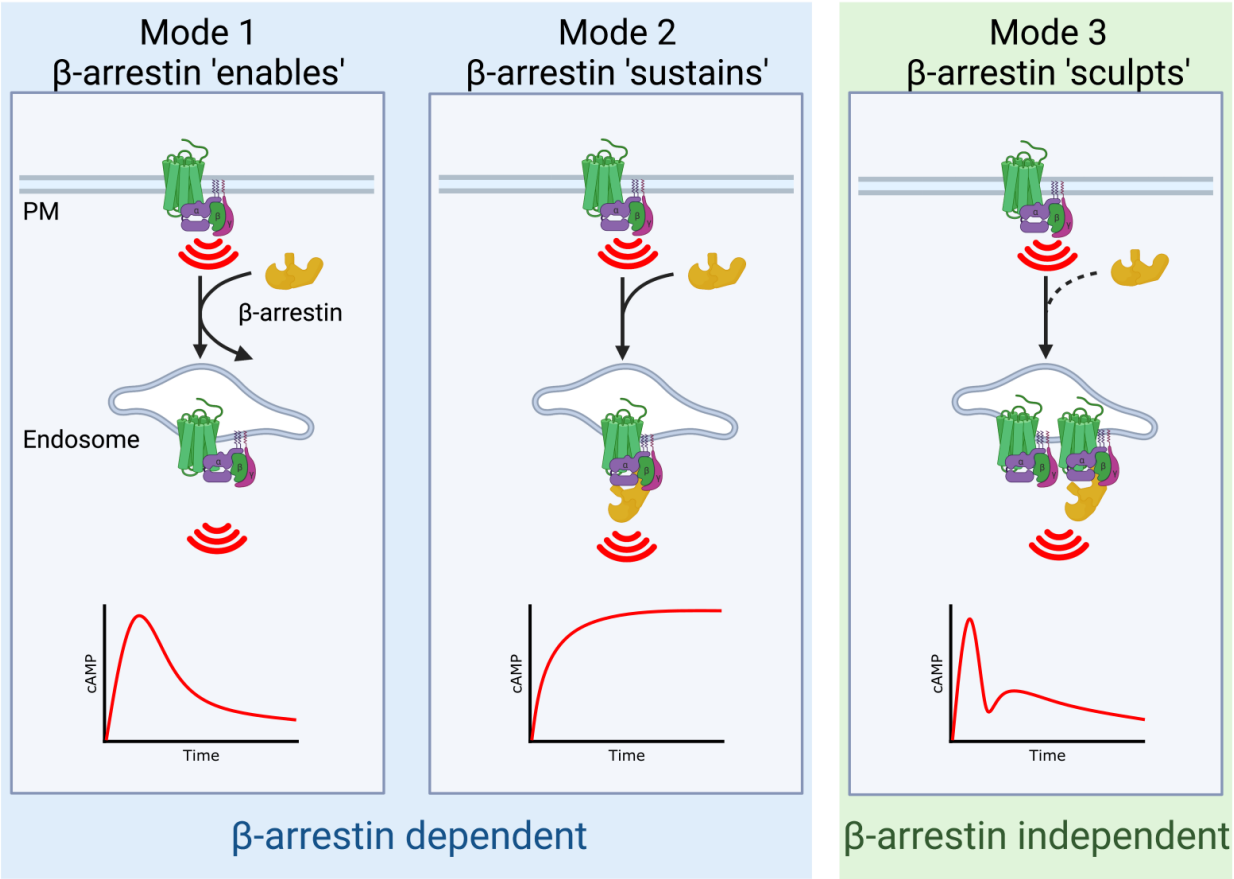

Figure 6. VIPR1 defines a third mode of endosomal GPCR signaling. Diagram illustrates key distinctions between signaling modes. A simplified representation of the temporal cAMP profile produced by each mode is plotted below. *Mode 1:* β-arrestin enables signaling from endosomes by promoting receptor internalization and then dissociating. *Mode 2:* β-arrestin promotes receptor internalization and then remains bound after internalization to form a signal-sustaining endosomal megaplex. *Mode 3:* β-arrestin is not required for receptor internalization or signaling from endosomes; instead, β-arrestin sculpts the resulting combined signal output, such that the plasma membrane and endosomal signal phases produce temporally resolved cAMP peaks. Schematic generated using Biorender.

Supplemental Figures and Tables

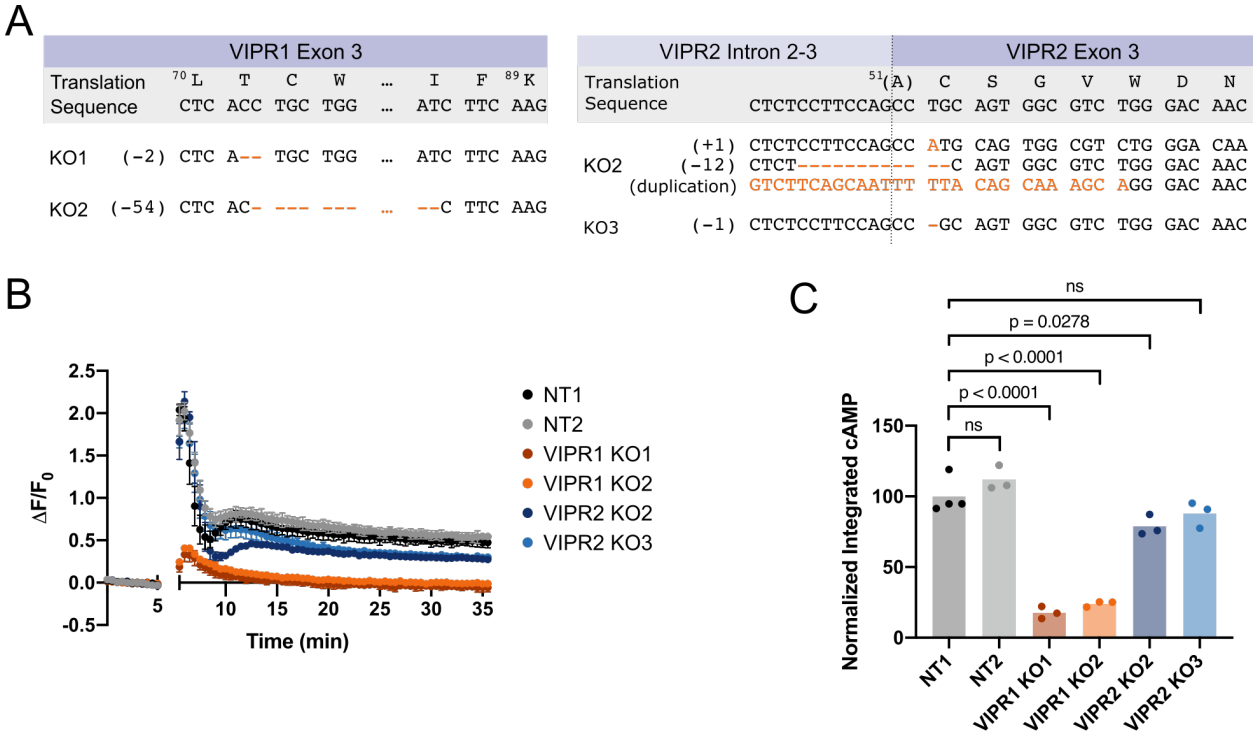

Supplementary Figure 1. Characterization of VIPR knockout (KO) cell lines. (A) Alignments showing the genetic modifications of VIPR1 and VIPR2 in independent monoclonal lines generated by CRISPR. (B) Fluorescence change of cADDis cAMP biosensor upon treatment with 500 nM VIP added at 5 minutes. NT1 and NT2 are polyclonal HEK293 cell lines treated with nontargeting sgRNAs. N ≥ 3 and error bars are S.D. (C) Integrated cAMP from (B), calculated as area under the curve and normalized to the average of NT1. Significance was determined by a one-way ANOVA with Dunnett's multiple comparisons test

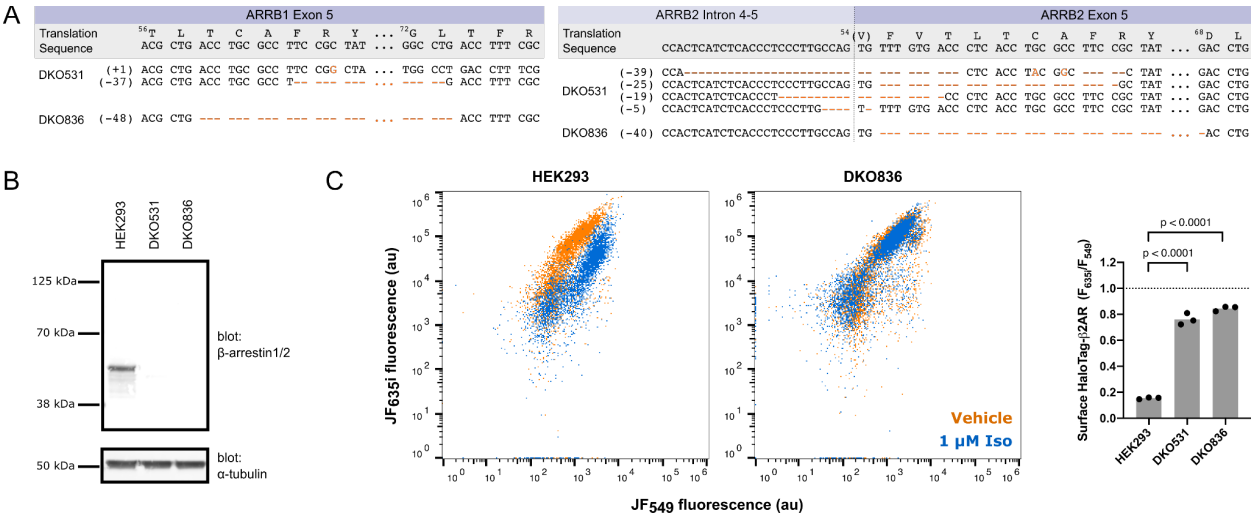

Supplementary Figure 2. Characterization of β-arrestin1/2 double knockout (β-arr1/2 DKO) cell lines DKO836 (main text figures) and DKO531 (supplemental figures). (A) Alignments showing the genetic modifications of β-arr1 (ARRB1) and β-arr2 (ARRB2) in independent monoclonal lines generated by CRISPR. (B) Western blot of parental HEK293 and β-arr DKO cell lysate, probing for β-arrestin1/2 and α-tubulin as a loading control. (C) Flow cytometry showing the agonist-induced internalization of the β2 adrenergic receptor (β2AR) in HEK293 and β-arr1/2 DKO cells. Cells stably overexpressing an N-terminal HaloTag fusion of β2AR were treated with 1 **μ**M isoproterenol (Iso), a β2AR agonist, or vehicle for 20 minutes. Receptors remaining on the surface were labeled with cell-impermeable JF_{635}i-HTL, after which all other receptors were labeled with the cell-permeable JFX_{549}xHTL. Representative dot plots of fluorescence with vehicle (orange) and Iso (blue) for HEK293 (right) and DKO836 (left) are shown. Surface receptor was calculated as a ratio of median fluorescence. Due to the high background with JFX_{549}xHTL, cells were gated for analysis to only include cells with receptor expression levels above background. Significance was determined by a one-way ANOVA with Dunnett's multiple comparisons test.

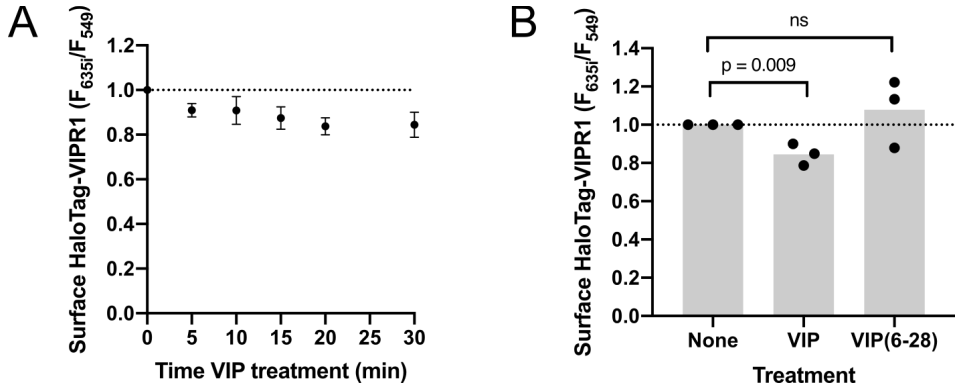

Supplementary Figure 3. VIP treatment modestly reduces surface VIPR1. (A) Timecourse of surface HaloTag-VIPR1 after 1 μM VIP treatment, as measured by flow cytometry. HEK293 cells stably expressing HaloTag-VIPR1 were exposed to VIP for the appropriate time, and the ratio of surface versus internal receptors was determined using cell-impermeable JF_{635}i-HTL and cell-permeable JFX_{549}-HTL as described in Methods. N = 3 and error bars are S.D. (B) Comparison of surface HaloTag-VIPR1 after 30 minute treatment with 1 μM VIP or VIP(6-28). Data for VIP treatment is repeated from (A). Significance was determined with unpaired t-tests.

469

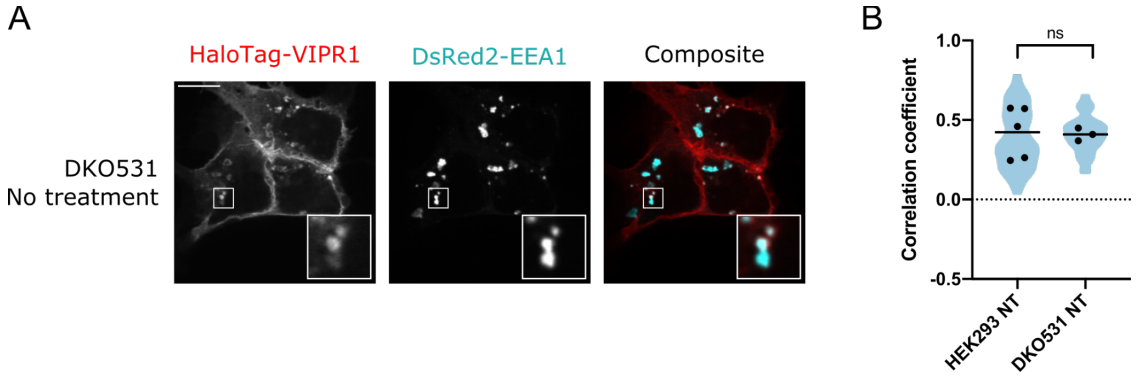

470
471

472 **Supplementary Figure 4.** VIPR1 is internalized in a β-arrestin-independent manner. (A) β-arr1/2
473 DKO531 cells coexpressing HaloTag-VIPR1, labeled with JF_{635}i-HTL for 10 minutes, and
474 DeRed2-EEA1 were fixed and imaged. (B) Quantification of fixed imaging in (A). Cells were
475 manually segmented, and the correlation coefficient was calculated for each cell. Mean correlation
476 coefficients are shown for each biological replicate (9-28 cells), with a line at the mean of means
477 and cell-level data superimposed as a violin plot. Untreated HEK293 data is repeated from Figure
478 2B. Significance was determined by a one-way ANOVA with Dunnett's multiple comparisons test
479 with the data shown in Figure 2B.

480

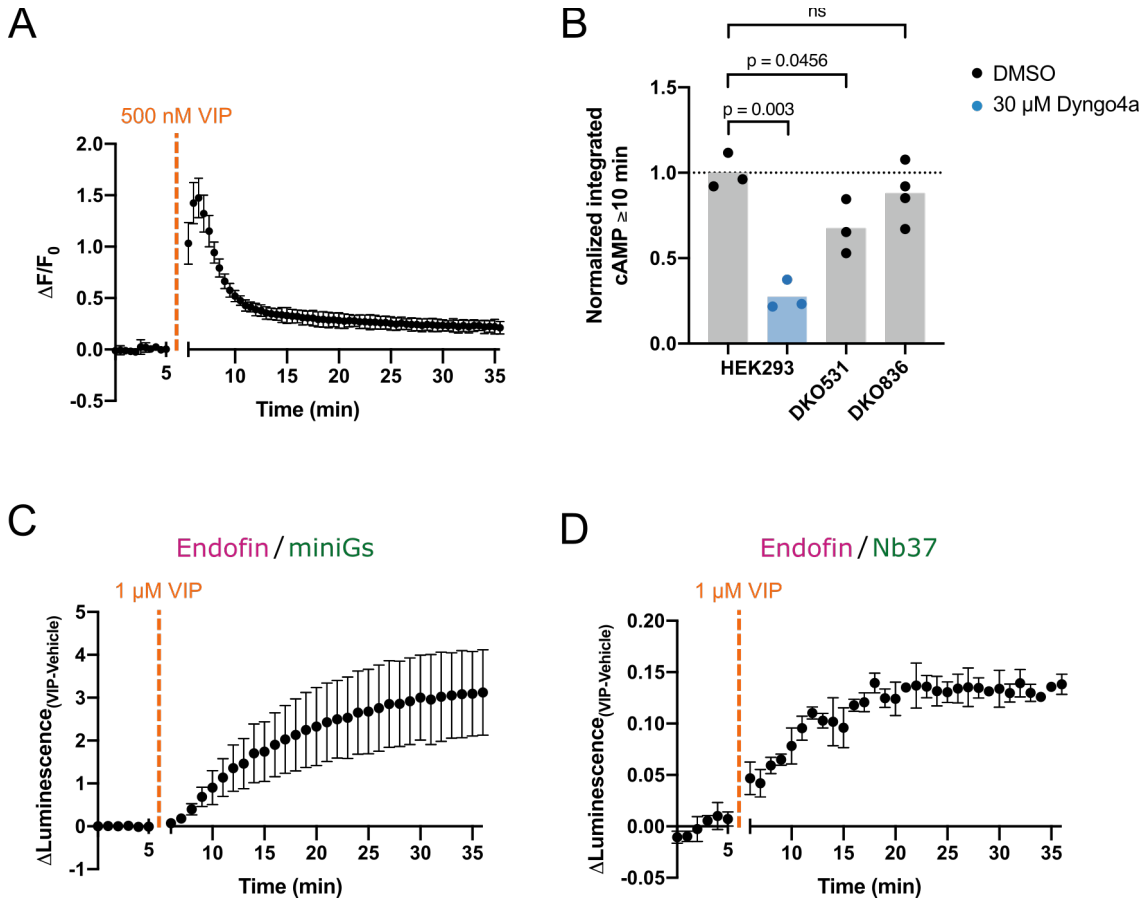

481
482

483 **Supplementary Figure 5.** Independent β-arr1/2 DKO cell line DKO531 recapitulates cAMP
484 signaling trends. (A) Fluorescence change of cADDis in DKO531 upon treatment with 500 nM VIP
485 added at 5 minutes. Compare to Figure 4A. (B) Normalized integrated cAMP from the second
486 phase of signaling, defined as 5-30 minutes after VIP addition (represented by points 10-35 min
487 in panel A, Figure 1A, and Figure 4A). Significance was determined by a one-way ANOVA test
488 with Dunnett's multiple comparisons test. (C, D) Change in luminescence in β-arr1/2 DKO cells
489 with endofin-LgBiT and SmBiT-miniGs (C) or Nb37-SmBiT (D) upon addition of 1 μM VIP at 5
490 minutes. Compare to Figure 4B-C. For all data, n ≥ 3 and error bars are S.D.

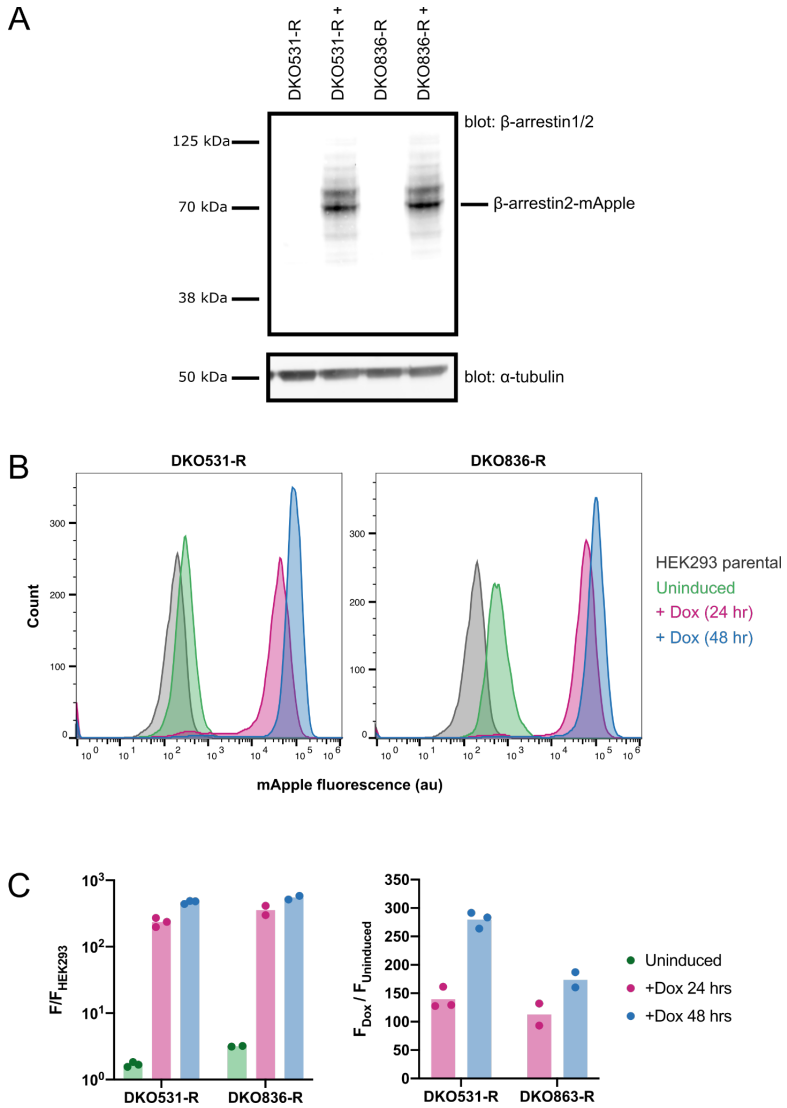

Supplementary Figure 6. Characterization of β-arr1/2 DKO rescue cell lines, DKO531-R and DKO836-R. (A) Western blot of β-arr1/2 DKO rescue cell lysates, probing for β-arr1/2 and α-tubulin as a loading control. Rescue cell lines stably express β-arr2-mApple under the control of a tet-inducible promoter (P_{TRE3GS}). Cells were induced with doxycycline (Dox) for 24 hours. (B) Representative flow cytometry data showing the expression of β-arr2 upon dox induction, as measured by mApple fluorescence. (C) Quantification of flow cytometry data shown in (B). Ratios of the median mApple fluorescence are shown compared to parental HEK293 cells (right) and the uninduced β-arr1/2 DKO-R cell lines (left).

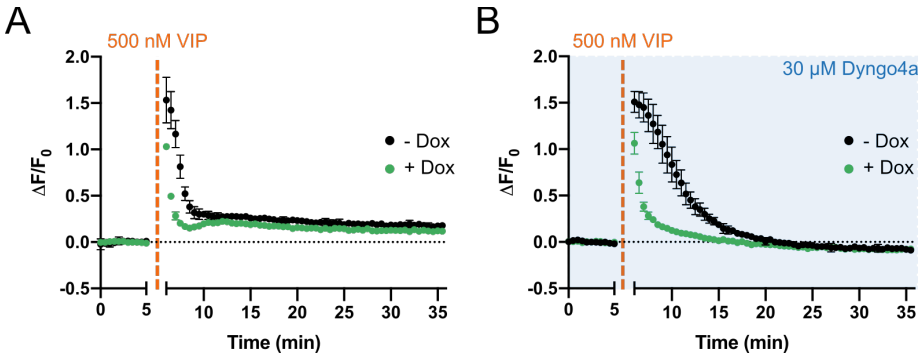

Supplementary Figure 7. Independent DKO rescue cell line DKO531-R recapitulates cAMP signaling trends. Fluorescence change of cADDis in DKO531-R upon treatment with 500 nM VIP added at 5 minutes. Cells were pretreated with DMSO (A) or 30 μM Dyngo4a (B) for 10 minutes. Compare to Figure 5A. Cells treated with dox to induce expression β-arr-mApple are shown in green, n ≥ 3, and error bars are S.D.

509 **Supplementary Tables.**

510

511 **Supplementary Table 1.** DNA constructs used in this study.

512

Construct	Source
pcDNA3_mCherry	This study: deletion of Dyn1 from pcDNA_mCherry-Dyn1[41]
pcDNA3_mCherry-Dyn1	[41]
pcDNA3_mCherry-Dyn1K44E	[41]
pCAGGS_LgBiT-CAAX	[42]
pCAGGS_endofin-LgBiT	[42]
pEGFP-βarr2-SmBiT	[43]
pcDNA3.1_SmBiT-miniGs	This study: insertion of miniGs[32] into pcDNA3.1 with SmBiT(114) added into primers.
pcDNA3.1_Nb37-SmBiT(101)	This study: insertion of Nb37 (from R. Irannejad) into pcDNA3.1 with SmBiT(101)[44] added into primers.
GNB1-T2A-cpVenus-GNGT1-IRES-GNAS	This study: deletion of Nluc from Gs(short)-CASE. Gs(short)-CASE was a gift from Gunnar Schulte (Addgene plasmid # 168124).
pcDNA3.1_SS-FLAG-VIPR1	This study: insertion of VIPR1(31-457) (from A. Marley) into pcDNA3.1 following the signal sequence of influenza hemagglutinin (SS) and FLAG-linker (MKTIIALSYIFCLVFADYKDDDDGGS)
pcDNA3.1_SS-HaloTag-VIPR1	This study: replacement of FLAG-linker with HaloTag7 in pcDNA3.1-SS-HaloTag-VIPR1
pcDNA_SS-HaloTag-β2AR	This study: replacement of FLAG with HaloTag7 in pcDNA_SS-FLAG-β2AR[45]
pDsRed2-EEA1(2xFYVE)	From R. Irannejad
pmApple_Arr2-mApple	[46]
pLVX-TetOne-Puro_Arr3-mApple	This study; insertion of Arr3-mApple[46] into pLVX-TetOne-Puro (Takara Bio).

513

514

515 **Supplementary Table 2.** CRISPR knockout cell line reagents.

Target	sgRNA sequence	Forward PCR validation primer(s)*	Reverse PCR validation primer(s)*	NGS primers
VIPR1	UGUGGGACAACCUCACCUGC	GTGAGCCTTTCCCACATGCTTATC	CAACAGTCAAAACCACCACTGGC	
VIPR2	UCCCAGACGCCACUGCAGGC	GAAGGCAGGTGATGCCCTTCT	CCAGTGGTGCCCATTTCATCACA	
ARRB1	GUCCUCCCGGCCAUAGCGGA	CATACCCCTCCACATATGCCC	GTCCCAGCATACACTGGGAAAC	
ARRB2 (DKO531 & DKO836)	CAGGUGAGGGUCACAAACAC	1. GGATGAGAAGGGAAGAAGGAAGG 2. CTGCCTCACTGTTTCTTCCAGATC	1. GACAAAGTGGACCCTGTAGGTAAG 2. CAGGAAGTGAGCTGGTGTGTC	Forward: ACACTCTTTCCCTACACGACGCTCTTCCGATCTAAGTGAAATGGGCTGGCCTTGG Reverse: GACTGGAGTTCAGACGTGTGCTCTTCCGATCTATGCTGGCCCAGCTTCCTCA
ARRB2	CCGCUAUGGCCGUGAAGACC	1. GGATGAGAAGGGAAGAAGGAAGG 2. CTGCCTCACTGTTTCTTCCAGATC	1. GACAAAGTGGACCCTGTAGGTAAG 2. CAGGAAGTGAGCTGGTGTGTC	
NT1	GCACUACCAGAGCUAA	NA	NA	
NT2	GUACGUCGGUAUAACU	NA	NA	

516 *Two sets of primers reflect nested PCR strategy

517 **References**

518

519 1. Hauser, A. S., Attwood, M. M., Rask-Andersen, M., Schiöth, H. B. & Gloriam, D. E. Trends
520 in GPCR drug discovery: new agents, targets and indications. *Nat. Rev. Drug Discov.* **16**,
521 829–842 (2017).

522 2. Sutkeviciute, I. & Vilardaga, J.-P. Structural insights into emergent signaling modes of G
523 protein–coupled receptors. *J. Biol. Chem.* **295**, 11626–11642 (2020).

524 3. Hilger, D., Masureel, M. & Kobilka, B. K. Structure and dynamics of GPCR signaling
525 complexes. *Nat. Struct. Mol. Biol.* **25**, 4–12 (2018).

526 4. Katritch, V., Cherezov, V. & Stevens, R. C. Structure-Function of the G Protein–Coupled
527 Receptor Superfamily. *Annu. Rev. Pharmacol. Toxicol.* **53**, 531–556 (2013).

528 5. Weis, W. I. & Kobilka, B. K. The Molecular Basis of G Protein–Coupled Receptor Activation.
529 *Annu. Rev. Biochem.* **87**, 897–919 (2018).

530 6. Calebiro, D. & Koszegi, Z. The subcellular dynamics of GPCR signaling. *Mol. Cell.*
531 *Endocrinol.* **483**, 24–30 (2019).

532 7. Lobingier, B. T. & von Zastrow, M. When trafficking and signaling mix: How subcellular
533 location shapes G protein-coupled receptor activation of heterotrimeric G proteins. *Traffic*
534 **20**, 130–136 (2019).

535 8. Hanyaloglu, A. C. & Zastrow, M. von. Regulation of GPCRs by Endocytic Membrane
536 Trafficking and Its Potential Implications. *Annu. Rev. Pharmacol. Toxicol.* **48**, 537–568
537 (2008).

538 9. Calebiro, D. *et al.* Persistent cAMP-Signals Triggered by Internalized G-Protein–Coupled
539 Receptors. *PLoS Biol.* **7**, e1000172 (2009).

540 10. Ferrandon, S. *et al.* Sustained cyclic AMP production by parathyroid hormone receptor
541 endocytosis. *Nat. Chem. Biol.* **5**, 734–742 (2009).

542 11. Kotowski, S. J., Hopf, F. W., Seif, T., Bonci, A. & von Zastrow, M. Endocytosis Promotes
543 Rapid Dopaminergic Signaling. *Neuron* **71**, 278–290 (2011).
544 12. Feinstein, T. N. *et al.* Retromer terminates the generation of cAMP by internalized PTH
545 receptors. *Nat. Chem. Biol.* **7**, 278–284 (2011).
546 13. Feinstein, T. N. *et al.* Noncanonical Control of Vasopressin Receptor Type 2 Signaling by
547 Retromer and Arrestin. *J. Biol. Chem.* **288**, 27849–27860 (2013).
548 14. Irannejad, R. *et al.* Conformational biosensors reveal GPCR signalling from endosomes.
549 *Nature* **495**, 534–538 (2013).
550 15. Merriam, L. A. *et al.* Pituitary Adenylate Cyclase 1 Receptor Internalization and Endosomal
551 Signaling Mediate the Pituitary Adenylate Cyclase Activating Polypeptide-Induced Increase
552 in Guinea Pig Cardiac Neuron Excitability. *J. Neurosci.* **33**, 4614–4622 (2013).
553 16. Tsvetanova, N. G. & von Zastrow, M. Spatial encoding of cyclic AMP signaling specificity by
554 GPCR endocytosis. *Nat. Chem. Biol.* **10**, 1061–1065 (2014).
555 17. Thomsen, A. R. B. *et al.* GPCR-G Protein-β-Arrestin Super-Complex Mediates Sustained G
556 Protein Signaling. *Cell* **166**, 907–919 (2016).
557 18. Lyga, S. *et al.* Persistent cAMP Signaling by Internalized LH Receptors in Ovarian Follicles.
558 *Endocrinology* **2016**, 63–71 (2016).
559 19. Godbole, A., Lyga, S., Lohse, M. J. & Calebiro, D. Internalized TSH receptors en route to
560 the TGN induce local Gs-protein signaling and gene transcription. *Nat. Commun.* **8**, (2017).
561 20. Cahill, T. J. *et al.* Distinct conformations of GPCR–β-arrestin complexes mediate
562 desensitization, signaling, and endocytosis. *Proc. Natl. Acad. Sci.* **114**, 2562–2567 (2017).
563 21. White, A. D. *et al.* Spatial bias in cAMP generation determines biological responses to PTH
564 type 1 receptor activation. *Sci. Signal.* **14**, eabc5944 (2021).
565 22. Oakley, R. H., Laporte, S. A., Holt, J. A., Caron, M. G. & Barak, L. S. Differential Affinities of
566 Visual Arrestin, βArrestin1, and βArrestin2 for G Protein-coupled Receptors Delineate Two
567 Major Classes of Receptors. *J. Biol. Chem.* **275**, 17201–17210 (2000).

568 23. Nguyen, A. H. *et al.* Structure of an endosomal signaling GPCR–G protein–β-arrestin
569 megacomplex. *Nat. Struct. Mol. Biol.* **26**, 1123–1131 (2019).
570 24. Wehbi, V. L. *et al.* Noncanonical GPCR signaling arising from a PTH receptor–arrestin–Gβγ
571 complex. *Proc. Natl. Acad. Sci.* **110**, 1530–1535 (2013).
572 25. Gidon, A. *et al.* Endosomal GPCR signaling turned off by negative feedback actions of PKA
573 and v-ATPase. *Nat. Chem. Biol.* **10**, 707–709 (2014).
574 26. Moo, E. V., van Senten, J. R., Bräuner-Osborne, H. & Møller, T. C. Arrestin-Dependent and
575 -Independent Internalization of G Protein–Coupled Receptors: Methods, Mechanisms, and
576 Implications on Cell Signaling. *Mol. Pharmacol.* **99**, 242–255 (2021).
577 27. Claing, A. *et al.* Multiple endocytic pathways of G protein-coupled receptors delineated by
578 GIT1 sensitivity. *Proc. Natl. Acad. Sci.* **97**, 1119–1124 (2000).
579 28. Shetzline, M. A., Walker, J. K. L., Valenzano, K. J. & Premont, R. T. Vasoactive Intestinal
580 Polypeptide Type-1 Receptor Regulation. *J. Biol. Chem.* **277**, 25519–25526 (2002).
581 29. Atwood, B. K., Lopez, J., Wager-Miller, J., Mackie, K. & Straiker, A. Expression of G protein-
582 coupled receptors and related proteins in HEK293, AtT20, BV2, and N18 cell lines as
583 revealed by microarray analysis. *BMC Genomics* **12**, 14 (2011).
584 30. Cho, N. H. *et al.* OpenCell: Endogenous tagging for the cartography of human cellular
585 organization. *Science* **375**, eabi6983 (2022).
586 31. Carpenter, B. & Tate, C. G. Engineering a minimal G protein to facilitate crystallisation of G
587 protein-coupled receptors in their active conformation. *Protein Eng. Des. Sel.*
588 proeng;gzw049v1 (2016) doi:10.1093/protein/gzw049.
589 32. Wan, Q. *et al.* Mini G protein probes for active G protein–coupled receptors (GPCRs) in live
590 cells. *J. Biol. Chem.* **293**, 7466–7473 (2018).
591 33. Westfield, G. H. *et al.* Structural flexibility of the G s -helical domain in the 2-adrenoceptor
592 Gs complex. *Proc. Natl. Acad. Sci.* **108**, 16086–16091 (2011).

593 34. Jonker, C. T. H. *et al.* Accurate measurement of fast endocytic recycling kinetics in real
594 time. *J. Cell Sci.* jcs.231225 (2019) doi:10.1242/jcs.231225.
595 35. Fishbein, V. A. *et al.* A chimeric VIP-PACAP analogue but not VIP pseudopeptides function
596 as VIP receptor antagonists. *Peptides* **15**, 95–100 (1994).
597 36. Dai, S. A. *et al. State-selective Modulation of Heterotrimeric Gαs Signaling with Macrocyclic*
598 *Peptides*. http://biorxiv.org/lookup/doi/10.1101/2020.04.25.054080 (2020)
599 doi:10.1101/2020.04.25.054080.
600 37. Edelstein, A. D. *et al.* Advanced methods of microscope control using μManager software.
601 *J. Biol. Methods* **1**, e10 (2014).
602 38. Stirling, D. R. *et al.* CellProfiler 4: improvements in speed, utility and usability. *BMC*
603 *Bioinformatics* **22**, 433 (2021).
604 39. Schindelin, J. *et al.* Fiji: an open-source platform for biological-image analysis. *Nat. Methods*
605 **9**, 676–682 (2012).
606 40. Grimm, J. B. *et al.* A General Method to Improve Fluorophores Using Deuterated
607 Auxochromes. *JACS Au* **1**, 690–696 (2021).
608 41. Peng, G. E., Pessino, V., Huang, B. & von Zastrow, M. Spatial decoding of endosomal
609 cAMP signals by a metastable cytoplasmic PKA network. *Nat. Chem. Biol.* **17**, 558–566
610 (2021).
611 42. Xu, Z. *et al.* Structural basis of sphingosine-1-phosphate receptor 1 activation and biased
612 agonism. *Nat. Chem. Biol.* **18**, 281–288 (2022).
613 43. Barsi-Rhyne, B., Manglik, A. & von Zastrow, M. *Discrete GPCR-triggered endocytic modes*
614 *enable β-arrestins to flexibly regulate cell signaling*.
615 http://biorxiv.org/lookup/doi/10.1101/2022.07.13.499995 (2022)
616 doi:10.1101/2022.07.13.499995.
617 44. Dixon, A. S. *et al.* NanoLuc Complementation Reporter Optimized for Accurate
618 Measurement of Protein Interactions in Cells. *ACS Chem. Biol.* **11**, 400–408 (2016).

619 45. Cao, T. T., Deacon, H. W., Reczek, D. & Bretscher, A. A kinase-regulated PDZ-domain
620 interaction controls endocytic sorting of the b2-adrenergic receptor. **401**, 5 (1999).
621 46. Eichel, K., Jullié, D. & von Zastrow, M. β-Arrestin drives MAP kinase signalling from clathrin-
622 coated structures after GPCR dissociation. *Nat. Cell Biol.* **18**, 303–310 (2016).
623